Proceedings of the ASME 2014 International Mechanical Engineering Congress and Exposition
IMECE2014
November 14-20, 2014, Montreal, Quebec, Canada

IMECE2014-36661

Temperature Measurements in Powder-Bed Electron Beam Additive Manufacturing

Steven Price*, James Lydon, Ken Cooper**, Kevin Chou***

* Department of Mechanical Engineering
The University of Alabama, Tuscaloosa, AL 35487, USA

** Additive Manufacturing Laboratory
Marshall Space Flight Center, Huntsville, AL 35812, USA

ABSTRACT

Thermal characteristics such as process temperatures and melt pool sizes offer important information in metal additive manufacturing (AM) technologies such as powder-bed electron beam additive manufacturing (EBAM). In this study, a near infrared (NIR) thermal imager was employed to acquire build surface process temperatures during EBAM fabrications using Ti-6Al-4V powder. Challenges in NIR temperature measurements for EBAM were tackled including compensating temperatures due to the transmission loss and estimating the emissivity of Ti-6Al-4V in its molten state. At a beam speed of about 728 mm/s, a beam current of about 7.2 mA and a diameter of 0.55 mm, the maximum process temperature is on the order of around 2700 °C, and the melt pools have dimensions of about 2.72 mm and 0.72 mm in length and width, respectively.

KEYWORDS: Electron beam additive manufacturing, Near Infrared, Temperature measurement

INTRODUCTION

Metal based additive manufacturing (AM) technologies, using powder bed fusion, is one of major groups that can produce full density, functional components. This group of technologies applies a high energy-intensity beam to melt powder and fuse into a solid part, layer by layer. Powder-bed electron beam additive manufacturing (EBAM) technology is one of such technologies that have been employed for different applications in aerospace and biomedical industries, etc. An EBAM machine reads data of a three-dimensional (3D) computer-aided design (CAD) model and lays down successive layers of metal powders as raw materials. These layers are then melted by utilizing an electron beam, and then self-cooled and rapidly solidified. EBAM is capable of producing high strength, full density metal parts unlike other AM methods such as selective laser sintering. Because of its high energy density, the EBAM fabrication process is much faster than other alternatives such as selective laser melting. EBAM enables the fabrication of metal parts with complex geometries such as fine network structures and internal channels and cavities that are difficult to produce using conventional manufacturing methods.

There are still many process challenges in EBAM due to lack of comprehensive understanding of the process physics, and there is an increasing interest in process modeling and simulations in EBAM. On the other hand, there is also a need for in-situ process measurements such as temperatures for model validation and process monitoring purposes. The ability to measure the temperatures that occur during the build process is an essential capability that must be established in order to verify process models, predict part microstructure, and develop feedback control systems [1]. There is little literature available that presents temperature measurement results from the EBAM process. Zäh and Lutzmann [2] placed thermocouples in the

build plate of an EBAM machine and measured the temperature response as the electron beam passed above. The measured temperatures were compared to a model developed by the authors and a marginal difference of only 26 K was found after calibrations. Schwerdtfeger et al. [3] presented a method which could have important implications for quality control in EBAM. The authors used a FLIR A320 infrared camera to capture images of different layers of Ti-6Al-4V parts in an Arcam A2 system. These infrared images were used to identify defects in each layer. Rodriguez et al. [4] also used an IR camera (FLIR SC645) to monitor the fabrication process of Ti-6Al-4V parts in an Arcam A2 machine. Temperature data was collected after the completion of each layer and was analyzed to provide feedback information to modify the build settings for the next layer. Dinwiddie et al. [5] developed a periscope system to enable observation of the build surface during the EBAM. By using different values of focus offset current, the authors were able to obtain various levels of porosity which were detectable using a FLIR SC-8200 midwave IR camera.

A more detailed literature review and explanation of the experimental setup used in this paper may be found in Price et al. [1], who conducted temperature measurements of the EBAM process using a near infrared (NIR) camera sensitive in the 0.78-1.08 μm spectral range. The temperatures during the preheating, contour melting, and hatch melting phases of layer fabrication were measured and two dimensional temperature profiles of the molten pool during hatch melting were generated. There are several challenges associated with using an optical sensor for temperature measurements in EBAM. First, the emissivity of the measured metal surface may not be known (at high temperatures, involving liquid state). Several glasses are used for the viewport window of an EBAM machine, which will reduce the transmission of radiation. A leaded glass is used to block x-ray radiation from the electron beam source. In addition, a high-strength vacuum glass (quartz) is used for withstanding the thermal stress caused by the large temperature gradient between inside and outside of the build chamber. These glasses result in substantial transmission losses in the infrared spectrum. Hence, common IR thermal cameras are not suitable for such an application. Price et al. (2012) [1] evaluated a near infrared (NIR) thermal imager to measure temperature distributions and history of a build part surface during the EBAM process. Moreover, during melting in the EBAM process, disassociated metal molecules will deposit and attach to surfaces around including glasses used for a viewport window. In general, a replaceable thin piece of glass (called sacrificial glass) is placed in front of the built-in viewport glasses in order to protect them from metallization. A mechanical shutter is positioned in front of the sacrificial glass and shields it from metallization while the shutter is closed. A lever next to the viewport allows the shutter to be manually opened, enabling the build surface to be observed and its temperatures measured.

When capturing images during the melting process the shutter must be opened which causes a metal film to be deposited on the surface of glass. This film causes further transmission losses. Figure 1 shows an example of metalized glass after one EBAM build. The mechanical shutter was opened frequently, though no record of the total exposed time. It can be seen that transmission is severely reduced even at the visible light range. Using the light bulb testing technique, the transmission loss around the dark region is 85% to 90% in the wavelength of NIR used. Figure 2 shows examples of NIR images acquired in the initial build (0.35 mm) and in the later part of the build (36.19 mm) in this experiment. A noticeable difference can be observed.

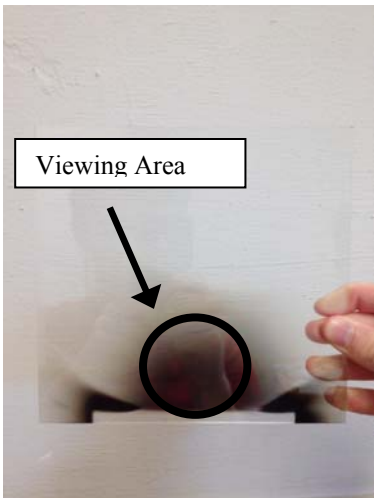

Figure 1. An example of a severely exposed sacrificial glass.

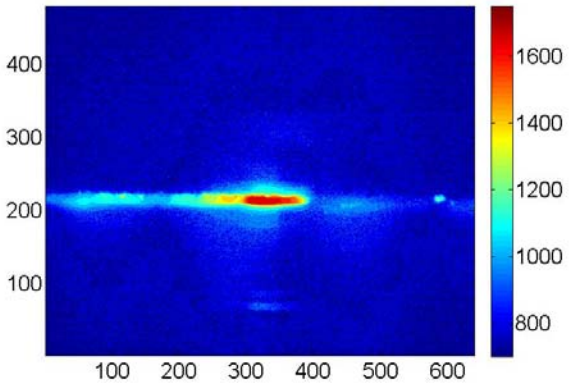

(a)

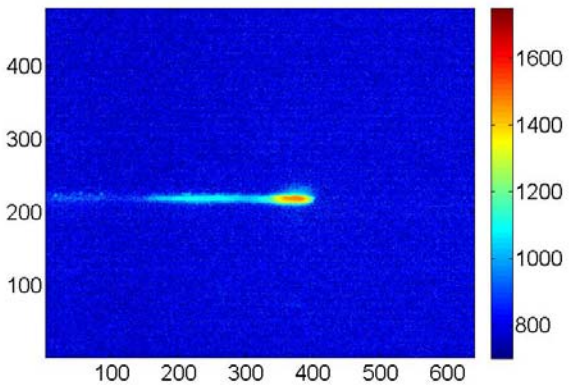

(b)

Figure 2. NIR images of hatch melting at build heights of (a) 0.35 mm and (b) 36.19 mm (Unit: °C).

Thermal contour images were further processed to extract temperature profiles along the beam moving direction, and across the beam center. Figure 3 compares temperature profiles at different build heights. During the entire build, the process parameters were kept constant (speed function 36). Very dramatic profile shifting can be observed. Though build height may result in profile shifting, however, not to this extent. It is suspected that the variable degree of metallization actually caused such a temperature profile difference because of large difference in transmission rate, which increases with exposure time.

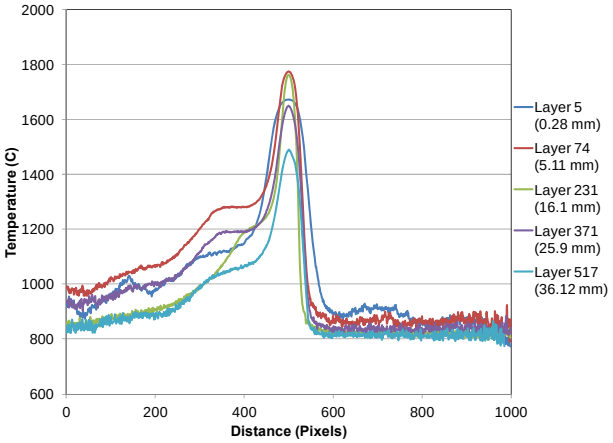

Figure 3. Average temperature profiles of the molten pool.

The objective of this research is to attempt temperature measurements in EBAM using an NIR thermal imager and to achieve better understanding of process temperatures that may be applied for the validation of EBAM thermal models. An NIR with a spectral range of 0.78-1.08 μm was employed to acquire thermal images during EBAM fabrications using Ti-6Al-4V powder. A CAD was designed and built to evaluate the spatial resolution and temperature distributions around a melt pool during melt scans. Post-processing data of NIR images was analyzed to quantify the maximum temperatures and melt pool sizes.

EXPERIMENTAL DETAIL

An Arcam S12 EBAM system, shown in Figure 4, at NASA's Marshall Space Flight Center (Huntsville, AL) was used to fabricate parts of a designed model in conjunction with temperature measurement experiments. Ti-6Al-4V powder from Arcam was used. The part designed for was a simple block: 50 mm long, 25 mm wide and 30 mm tall ($x \times y \times z$), with notches on the edge along the build direction, shown in Figure 5. The EBAM primary settings used were default values typically employed for Ti-6Al-4V powders. The layer thickness was 0.07 mm. A set of parameters called a build theme are suggested to dynamically control the electron beam speed and current as well as the raster spacing during the part fabrication process. These parameters are known as the speed functions and the purpose is to achieve and maintain the desired melt pool size. Additionally, the focus offset current is an influential parameter that controls the electron beam diameter [6].

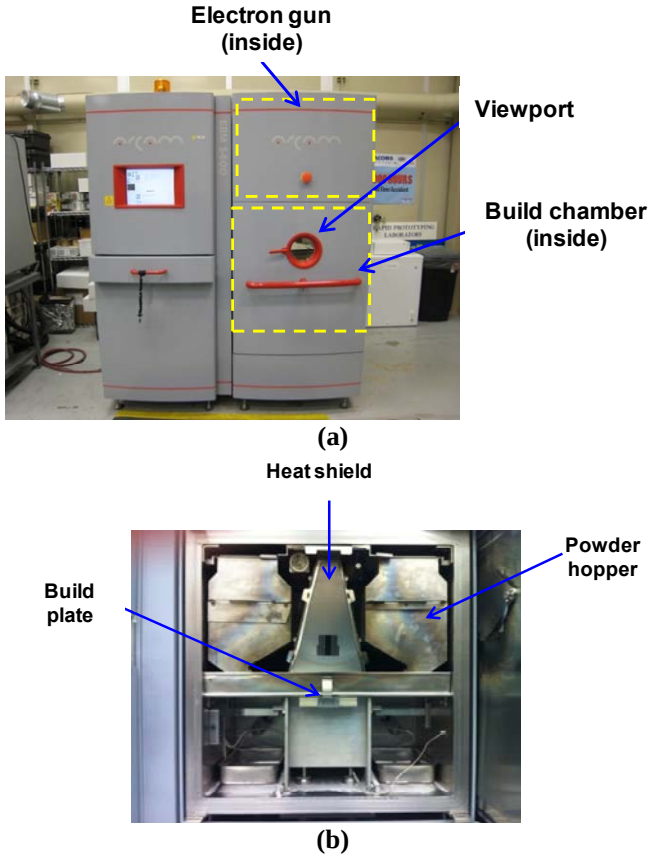

Figure 4. EBAM Machine: (a) overall outside, and (b) inside of the build chamber.

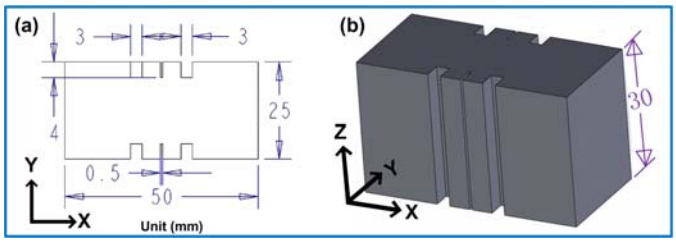

Figure 5. CAD model used in EBAM fabrications and temperature measurements.

A LumaSense MCS640 NIR camera was used to acquire dynamic spatial temperature distribution of the build surface during the EBAM fabrication process described above. The NIR camera has a spectral range of 0.78 to 1.08 μm and a 640 x 480 pixel focal plane array sensor. The image capturing system has a maximum frame rate of 60 Hz and a detectable temperature range of 600 °C to 3000 °C, which requires to be set as 3 different temperature ranges: low, medium and high, for separate calibrations. During each time of video acquisition, only one temperature can be selected and used, the high temperature range for melting scans. A lens with a minimal 500 mm working distance with a view area of 31 mm by 23 mm at 500 mm distance was used together. The NIR imager was calibrated together with the same glasses (leaded glass and quartz) in the viewport window, where the NIR will image

through, of the EBAM machine to obtain the transmission rate of the glasses. The emissivity of Ti-6Al-4V at high temperatures including over melting was not known, not reported. An assumed emissivity of 0.35 was used as the required single value setting of the NIR. The integration time of the image capturing system is 50 μs for the high temperature ranges. The NIR camera was mounted on a tripod and positioned to look downward through the EBAM machine's viewport onto the build platform, shown in Figure 6 shows the setup of the NIR in reference to the EBAM system for measurements. The NIR was vertically inclined at approximately 35°.

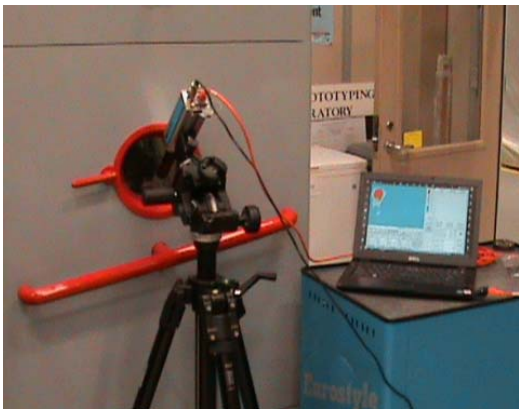

(a)

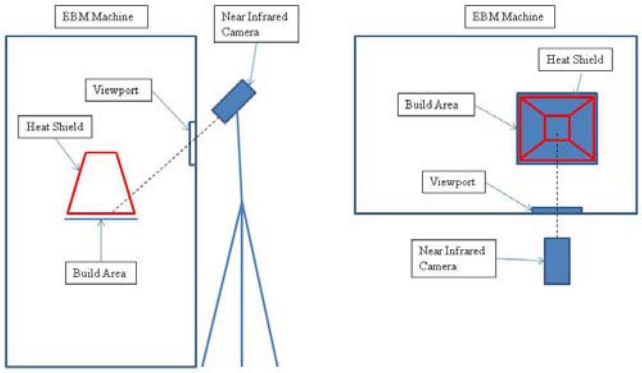

(b)

Figure 6. (a) NIR thermal imager setup and (b) A sketch showing position and orientation of the camera relative to the EBAM machine [1].

There are several challenges associated with using an optical sensor for temperature measurements in EBAM. First, the emissivity of the measured metal surface may not be known (at high temperatures, involving liquid state). In addition, during melting in the EBAM process, disassociated metal molecules will deposit and attach to surfaces around including glasses used for a viewport window. In general, a replaceable thin piece of glass (called sacrificial glass) is placed in front of the built-in viewport glasses in order to protect them from metallization. A mechanical shutter is positioned in front of the sacrificial glass and shields it from metallization while the shutter is closed. A lever next to the viewport allows the shutter to be manually opened, enabling the build surface to be observed and its temperatures measured.

The spatial resolutions of the NIR images were determined by identifying and measuring the distance between part features (included in the model design) observed during contour melting. An example binary image used for feature identification is shown in Figure 7. The blue lines indicate the identified edges and the red lines indicate the distances measured. In order to characterize the thermal behaviors during the electron beam scanning and melting, two-dimensional temperature profiles along the scanning paths were extracted from acquired NIR images. Statistical data was obtained and the signal/noise ratio was reduced by averaging all temperature profiles from all individual images acquired from a single layer build. The standard deviation of each location along the temperature profile was calculated to examine the repeatability of the temperature measurements from the experiments.

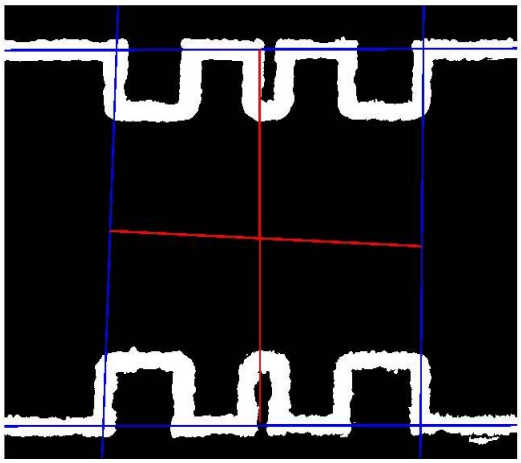

Figure 7. Contour melting data used for spatial resolution analysis.

During melting, if the viewport glass is exposed, the sacrificial glass will become covered with metal particles that reduce the transmission rate in the NIR. The transmission loss due to the metallization causes the measured temperatures to appear cooler than their true values. In order to better understand and compensate for the transmission loss, its effects on the temperature measurements were studied using the following approach. During one experiment of an EBAM build, the half of the sacrificial glass was covered to protect it from metallization. After this build, the transmission loss was evaluated. The protection cover was then removed and the same sacrificial glass now with known different transmission rate difference was used in the next experiment of an EBAM build of the same setup as the first experiment. The temperature images and profiles observed under each transmission rate were compared in order to analyze how the metallization affects the temperature measurement results. Since the severity of the metallization increases with amount of the exposure the sacrificial glass subjected to, the severity of the transmission loss increases as well. Therefore, the metallization effect on the measured temperatures at various build heights can be quantified. Based on the information obtained, the temperature

profiles were compensated to account for the transmission loss due to the metallization at that particular point in the build process.

The emissivity used in the NIR setting was a rough estimate. The true emissivity was estimated by comparing the measured apparent liquidus temperature compensated for transmission loss with the true liquidus temperature of Ti-6Al-4V, 1655 °C. Once the true emissivity had been found, the temperatures of the profile compensated for transmission loss were adjusted to reflect their values if the emissivity had been set to the true value. The molten pool length was then determined by finding the distance between the liquidus temperature on the heating and cooling size of the temperature profile. The molten pool width was determined in the same manner from a temperature profile made perpendicular to the scanning direction and intersecting the molten pool center.

Since the translational speed of the electron beam is controlled by a speed function (SF) algorithm, a machine-specific setting, its magnitude changes too as the build height increases. Thus, it was necessary to experimentally determine the beam speed in order that the same process parameters could be used in the simulation case to be verified. The beam speed was calculated by determining the distance travelled by the molten pool between two consecutive NIR images. Since the frame rate of the NIR camera and the spatial resolutions of the images were known, the beam speed could be calculated.

RESULTS AND DISCUSSION

An example of typical temperature images from NIR during hatch melting is shown in Figure 8(a). This particular example was at a build height of 26.53 mm. The electron beam translation speed was 632.6 mm/s and the beam current was 6.7 mA. By converting the NIR image in a binary image with the threshold of the measured liquidus temperature, it is possible to visualize the shape and size of the molten pool.

In order to characterize the thermal behavior during electron beam melting, two-dimensional temperature profiles along the scanning paths were extracted from acquired NIR images, an example from case described above is shown in Figure 8(b). The two-dimensional temperature profiles resemble the characteristics from a moving heat source phenomenon: large thermal gradients in the heating and cooling sides of the scanning paths. In addition, the phase transition region, liquidus to solidus, is evident as from the simulation. The raw temperature profiles from individual NIR images were noisy in the low temperature region, limited by the temperature detectable range. In order to obtain statistical information and reduce the signal/noise ratio, every temperature profile from all individual images acquired from a single layer build were averaged with the standard deviation calculated. An example of averaged temperature profile with standard deviation from at a build height of 26.53 mm is shown in Figure 8(c).

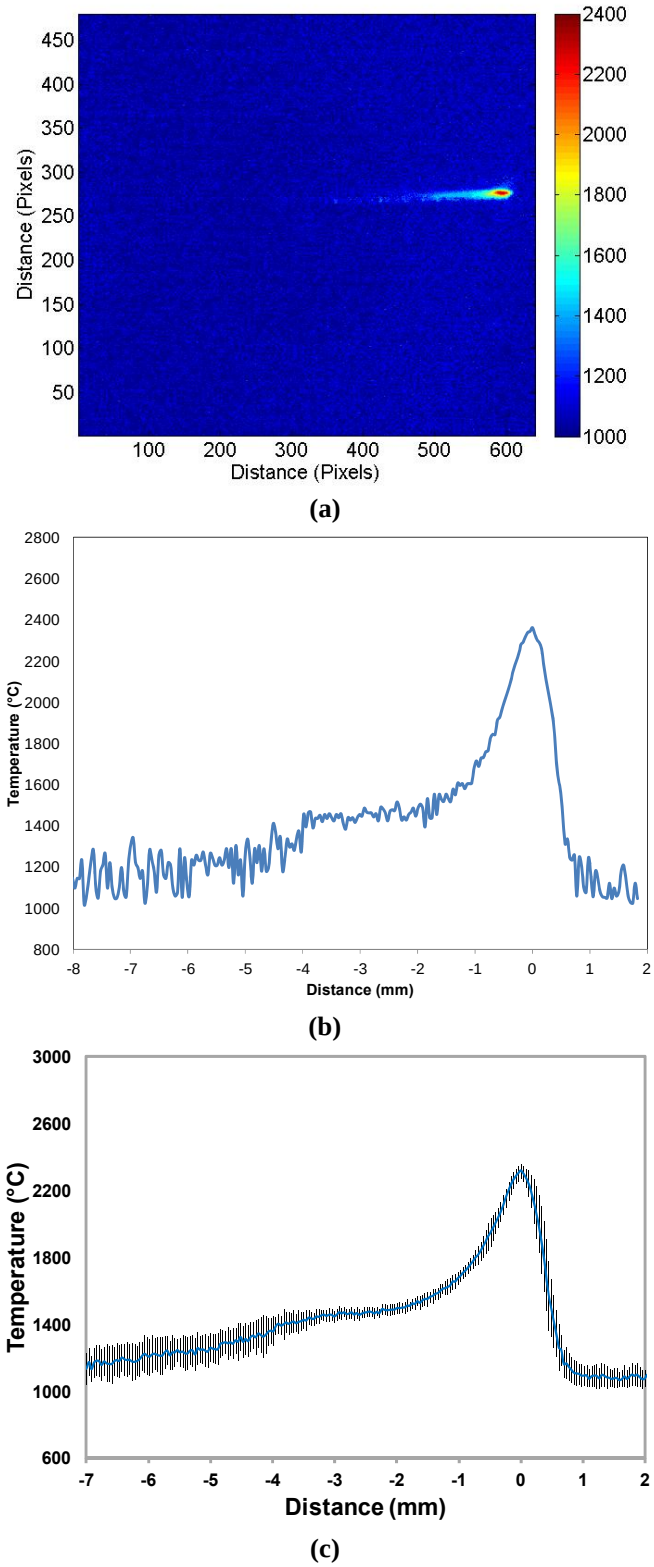

Figure 8. Typical NIR result from EBAM: (a) temperature contour with insert showing melt pool size, (b) temperature profile (c) average temperature profile with standard deviation.

As explained earlier, because of transmission loss due to metallization and uncertainty of the emissivity of the molten pool, the measured temperatures appeared lower than their true

values. A technique was developed to compensate for the transmission loss as well as identify the true emissivity and convert the temperatures to reflect their values at the true emissivity. Post-process analysis of temperature profiles, Figure 8(b), indicates that the measured liquidus temperature is low, which is due to the emissivity. Since, an assumed emissivity value, 0.35, was used in the NIR setting, it is necessary to convert the measured apparent temperatures to true temperatures, with a better approximated emissivity. in the experiment.

Equation (1) below is a modification of Plank's equation that describes the radiance of a black body at a certain wavelength as a function of the true temperature [7]. An unknown quantity may be determined by substituting known values of other variables and adjusting the unknown value until M is minimized. This equation can be applied to determine one of the apparent temperature, the true temperature and the emissivity when the other two variables are known. Therefore, Equation (1) was used to both convert temperatures from one emissivity to another and also to calculate the true emissivity.

$$M = \left| \left[\int_{\lambda_1}^{\lambda_2} \frac{w_\lambda}{\lambda^5 \left(\frac{c_2}{e^{\lambda \cdot T_{app}}} - 1 \right)} d\lambda \right] - \left[\varepsilon \int_{\lambda_1}^{\lambda_2} \frac{w_\lambda}{\lambda^5 \left(\frac{c_2}{e^{\lambda \cdot T_{true}}} - 1 \right)} d\lambda \right] - \left[(1-\varepsilon) \int_{\lambda_1}^{\lambda_2} \frac{w_\lambda}{\lambda^5 \left(\frac{c_2}{e^{\lambda \cdot T_{envir}}} - 1 \right)} d\lambda \right] \right|, \quad (1)$$

M = variable to minimize by adjusting other variables,
λ_1 = bottom of infrared camera's spectral range in µm,
λ_2 = top of infrared camera's spectral range in µm,
λ = wavelength of light in µm,
w_λ = relative sensitivity of camera at wavelength λ,
c_2 = second radiation constant (14388 µm·K),
T_{app} = apparent temperature in K,
T_{true} = true temperature in K,
T_{envir} = surrounding environment temperature in K,
and
ε = emissivity.

The measured liquidus temperature was used as the true temperature and the assumed emissivity value into the NIR setting was used as the emissivity input. The relative sensitivity of the camera at λ, w_λ, was assumed to be one. The surrounding environment temperature was assumed to be the room temperature. The equation was numerically solved for a range of apparent temperatures. The apparent temperature that resulted in the smallest value of M was the correct value. Next, using the calculated apparent temperature for the apparent temperature and the true liquidus temperature of Ti-6Al-4V for the true temperatures, the equation was numerically solved again, this time solving for the emissivity that resulted in the smallest value of M. This emissivity was the true emissivity of the Ti-6Al-4V molten pool. Current literature reporting values of the emissivity of T-6Al-4V was reviewed in order to determine a reasonable value to use during the experiment. González-Fernández et al. [8] investigated the spectral emissivity at an angle normal to the part surface of polished Ti-6Al-4V discs using a high accuracy infrared radiometer sensitive in the medium infrared spectrum. They found that the emissivity increased from around 0.1 to 0.35 at various temperatures as the wavelength dropped from 22 µm to 2.8 µm. Li [9], on the other hand, determined the hemispherical total emissivity of a Ti-6Al-4V sample suspended by electrostatic levitation by using a single color pyrometer sensitive at 700 nm. The author found that the emissivity of liquid Ti-6Al-4V at its melting temperature was 0.304, when using a heat capacity of 931 J/kg·K from literature.

An experimental procedure, describe earlier, was developed that would result a sacrificial glass to have two different levels of metallization, shown in Figure 9. A comparison of the measured temperatures of the molten pool as observed through both levels of metallization allowed the effects of the metallization on temperature measurements to be studied. The left half of the sacrificial glass was covered with a plastic film during the first build in order to protect it from metallization and a part was fabricated. When the build was completed, the transmission loss due to metallization was measured using a simple light bulb setup with NIR temperature measurements with adjusted transmission rate setting. The protective film was removed from the left side of the glass and it was returned to the machine and a second identical build was conducted. Thermal images were acquired from both sides of the glass. Figure 10 shows an example of temperature contours from the dark and light sides during one layer build. Two average temperature profiles were generated for each layer that was imaged, one from each side of the glass, Figure 11. These profiles were then compared to examine the effects of the different levels of metallization with the transmission loss corresponding to both sides also measured.

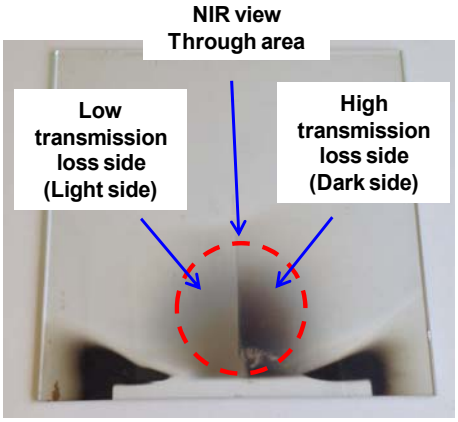

Figure 9. Sacrificial glass with two levels of metallization.

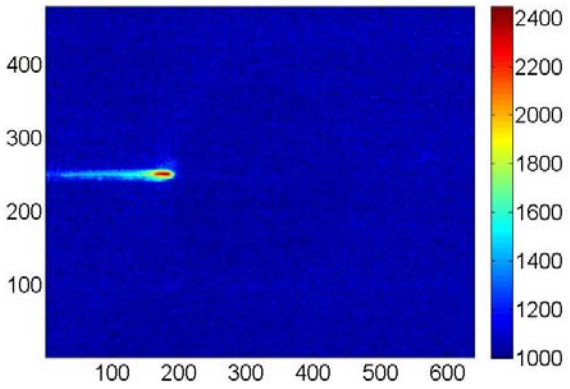

(a)

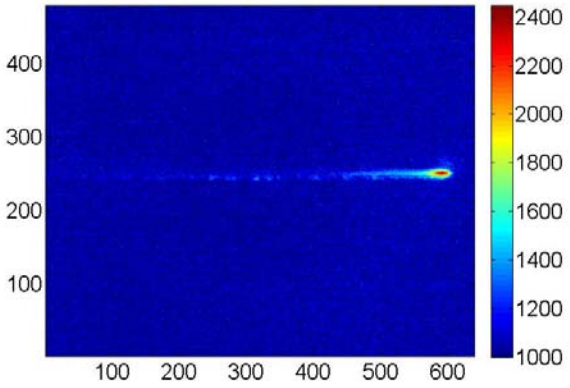

(b)

Figure 10. Thermal images from the same acquisition at one build height: (a) light side, and (b) dark side.

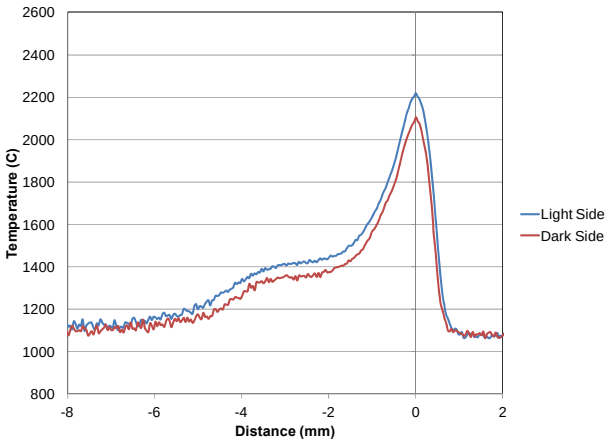

Figure 11. Temperature profiles from the same acquisition, but different transmission rates (build height of 26.39 mm).

By comparing the temperatures of the 2D temperature profiles from the lighter and darker sides of the sacrificial glass, it was possible to study how the transmission loss affected a range of temperatures. The transmission loss due to metallization was found to affect the temperatures near linearly, shown in Figure 12(a); therefore a method to compensate for the transmission loss was able to be developed. By assuming the emissivity of the molten pool, e.g. 0.28, a slope was calculated that would convert the measured liquidus temperature to the temperature that would result in a calculated emissivity of 0.28. This slope was found at various build heights from the experiment and the results are shown in Figure 12(b). After a temperature profile had been compensated for transmission loss, the true emissivity of the molten pool could be estimated using Equation (1) and then be used to convert the entire temperature profile. The average temperature profile from the experiment at a build height of 26.53 mm was compensated for transmission loss due to metallization. The emissivity was also recalculated using the method described above and the temperature profile was adjusted to reflect the values at true emissivity. The uncompensated, compensated for transmission loss, and compensated for transmission loss and emissivity adjustment temperature profiles are compared in Figure 13. Both compensations increased the temperatures; however, the transmission loss compensation had a larger effect. The effects of both compensations were also more significant at higher temperatures.

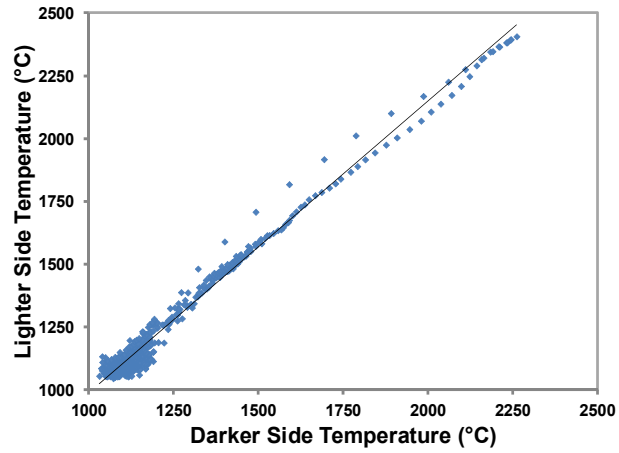

(a)

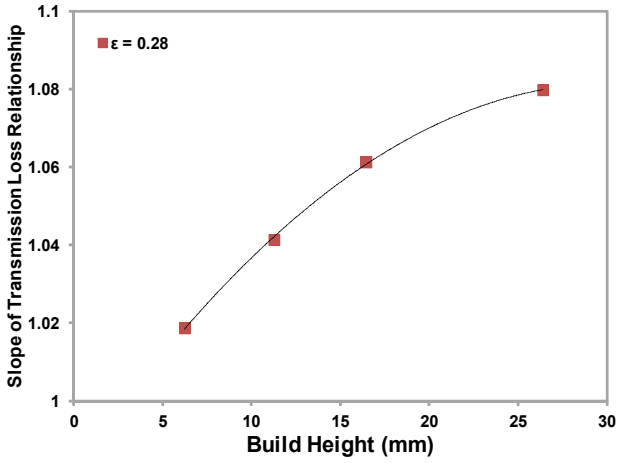

(b)

Figure 12. (a) Temperature difference due to transmission loss, and (b) transmission loss slope vs. build height.

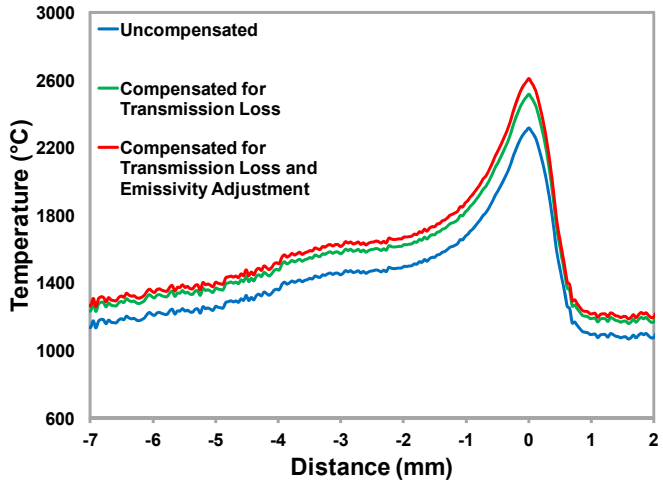

Figure 13. Temperature profiles showing before and after compensations.

In order to show the repeatability of the compensated temperature measurements, the temperature profiles from two different experiments, but with similar process parameters (a beam speed of 728 mm/s, a beam current of 7.2 mA, and a diameter of 0.55 mm,) were averaged together. This average temperature profile is shown in Figure 14 with the range of the standard deviations of the two profiles shown with error bars. The average dimensions of melt pools have a length of 2.72 mm and a width of 0.72 mm,

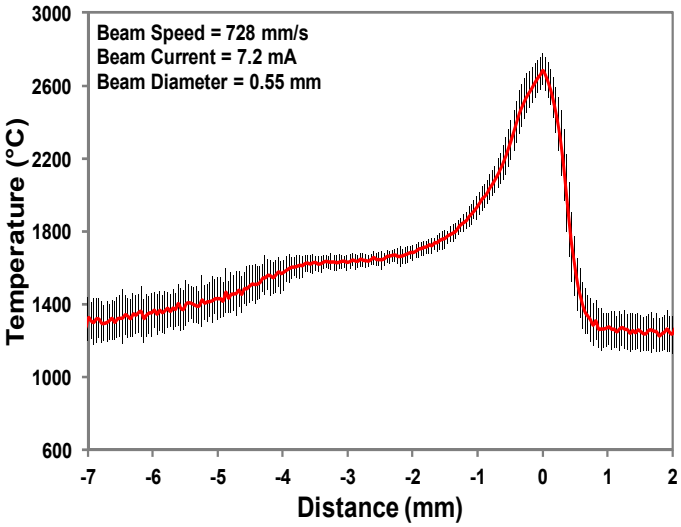

Figure 14. Average compensated temperature profile from two different experiments, showing range of standard deviations.

CONCLUSIONS

In this study, an NIR thermal imager was employed to measure the build surface temperatures during EBAM fabrications using Ti-6Al-4V powder. Challenges in NIR temperature measurements for EBAM were tackled including compensating temperatures due to the transmission loss and estimating the emissivity of Ti-6Al-4V in a molten state. A method was further developed to further analyze temperature profiles and melt pool sizes. The results show that at a beam speed of 728 mm/s, a beam current of 7.2 mA, and a diameter of 0.55 mm, the maximum temperatures in EBAM using Ti-6Al-4V powder are on the order around 2700 °C, and the melt pools have dimensions of about 2.72 mm and 0.72 mm in length and width, respectively.

ACKNOWLEDGMENT

This research is supported by NASA, No. NNX11AM11A, and is in collaboration with Marshall Space Flight Center (Huntsville, AL).

REFERENCES

[1] Price, S., Cooper, K., and Chou, Y. K., 2012, "Evaluations of Temperature Measurements by Near-Infrared Thermaography in Powder-Based Electron-Beam Additive Manufacturing," 23rd Annual International Solid Freeform Fabrication Symposium - An Additive Manufacturing Conference, Austin, TX, USA, August 6-8, 2012.

[2] Zäh, M. F., and Lutzmann, S., 2010, "Modelling and simulation of electron beam melting," Production Engeering. Research and Development, 4, pp. 15-23.

[3] Schwerdtfeger, J., Singer, R. F., and Körner, C., 2012, "In situ flaw detection by IR-imaging during electron beam melting," Rapid Prototyping Journal, 18(4), pp. 259-263.

[4] Rodriguez, E., Medina, F., Espalin, D., Terrazas, C., Muse, D., Henry, C., MacDonald, E., and Wicker, R.B., 2012, "Integration of a Thermal Imaging Feedback Control System in Electron Beam Melting," 23rd Annual International Solid Freeform Fabrication Symposium - An Additive Manufacturing Conference, Austin, TX, USA, August 6-8, 2012.

[5] Dinwiddie, R. B., Dehoff, R. R., Lloyd, P. D., Lowe, L. E., and Ulrich, J. B., 2013, "Thermographic In-Situ Process Monitoring of the Electron Beam Melting Technology used in Additive Manufacturing," SPIE Defense, Security, and Sensing, International Society for Optics and Photonics.

[6] Gong, H., Rafi, K., Starr, T., and Stucker, B., 2013, "The Effects of Processing Parameters on efect Regularity in Ti-6Al-4V Parts Fabricated By Selective Laser Melting and Electron Beam Melting," 24rd Annual International Solid Freeform Fabrication Symposium - An Additive Manufacturing Conference, Austin, TX, USA, August 12-14, 2013.

[7] Whitenton, E., 2010, "High-speed dual-spectrum imaging for the measurement of metal cutting temperatures," (No. NISTIR 7650), National Institute of Standards and Technology.

[8] González-Fernández, L., Risueño, E., Pérez-Sáez, R., and Tello, M., 2012, "Infrared normal spectral emissivity of Ti–6Al–4V alloy in the 500–1150K temperature range," Journal of Alloys and Compounds, 541, pp. 144-149.

[9] Li, J. J., 2009, "Study of liquid metals by electrostatic levitation," Ph.D. thesis, California Institute of Technology, Pasadena, CA.